Studying the impact of the nucleon size in relativistic heavy-ion collisions

Estudando o impacto do tamanho do núcleon em colisões de íons pesados relativísticos

Ficha catalográfica
Universidade Estadual de Campinas
Biblioteca do Instituto de Física Gleb Wataghin
Lucimeire de Oliveira Silva da Rocha - CRB 8/9174

Picchetti, João Paulo, 1996-
P581s Studying the impact of the nucleon size in relativistic heavy-ion collisions / João Paulo Picchetti. – Campinas, SP : [s.n.], 2022.

Orientador: Jun Takahashi.
Dissertação (mestrado) – Universidade Estadual de Campinas, Instituto de Física Gleb Wataghin.

1. Fenomenologia de íons pesados. I. Takahashi, Jun, 1971-. II. Universidade Estadual de Campinas. Instituto de Física Gleb Wataghin. III. Título.

Informações Complementares

Título em outro idioma: Estudando o impacto do tamanho do núcleon em colisões de íons pesados relativísticos
Palavras-chave em inglês:
Heavy ion phenomenology
Área de concentração: Física
Titulação: Mestre em Física
Banca examinadora:
Jun Takahashi [Orientador]
Márcio José Menon
Fernando Gonçalves Gardim
Data de defesa: 14-10-2022
Programa de Pós-Graduação: Física

Identificação e informações acadêmicas do(a) aluno(a)
- ORCID do autor: https://orcid.org/0000-0003-3273-9726
- Currículo Lattes do autor: http://lattes.cnpq.br/1916017801085456

MEMBROS DA COMISSÃO JULGADORA DA DISSERTAÇÃO DE MESTRADO DO ALUNO JOÃO PAULO PICCHETTI – RA 265948 APRESENTADA E APROVADA AO INSTITUTO DE FÍSICA “GLEB WATAGHIN”, DA UNIVERSIDADE ESTADUAL DE CAMPINAS, EM 14/10/2022.

COMISSÃO JULGADORA:

- Prof. Dr. Jun Takahashi – Presidente e orientador (IFGW/UNICAMP)
- Prof. Dr. Márcio José Menon (IFGW/UNICAMP)
- Prof. Dr. Fernando Gonçalves Gardim (UNIFAL-MG)

OBS: Ata da defesa com as respectivas assinaturas dos membros encontra-se no SIGA/Sistema de Fluxo de Dissertação/Tese e na Secretaria do Programa da Unidade.

CAMPINAS

2022

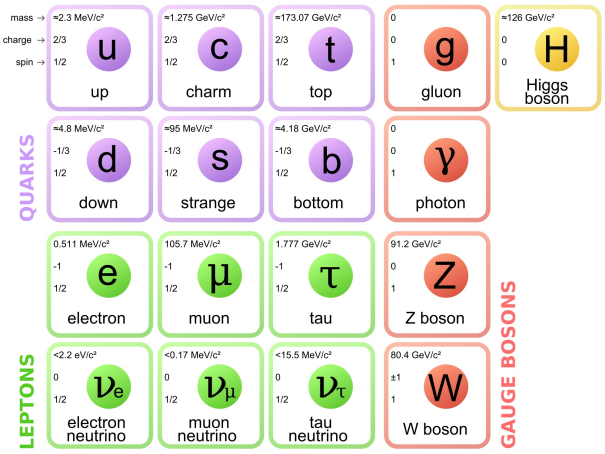
mass →
charge →
spin →
≈2.3 MeV/c²
2/3
1/2
u
up
≈1.275 GeV/c²
2/3
1/2
c
charm
≈173.07 GeV/c²
2/3
1/2
t
top
0
0
1
g
gluon
≈126 GeV/c²
0
0
H
Higgs boson
QUARKS
≈4.8 MeV/c²
-1/3
1/2
d
down
≈95 MeV/c²
-1/3
1/2
s
strange
≈4.18 GeV/c²
-1/3
1/2
b
bottom
0
0
1
γ
photon
0.511 MeV/c²
-1
1/2
e
electron
105.7 MeV/c²
-1
1/2
μ
muon
1.777 GeV/c²
-1
1/2
τ
tau
91.2 GeV/c²
0
1
Z
Z boson
GAUGE BOSONS
LEPTONS
<2.2 eV/c²
0
1/2
νe
electron neutrino
<0.17 MeV/c²
0
1/2
νμ
muon neutrino
<15.5 MeV/c²
0
1/2
ντ
tau neutrino
80.4 GeV/c²
±1
1
W
W boson

	✓	✓	✓
		✓	✓
			✓

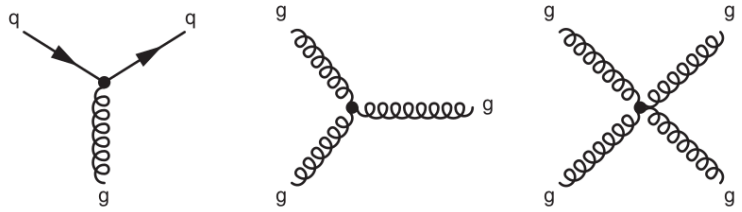
q
q
g
g
g
g
g
g
g
g

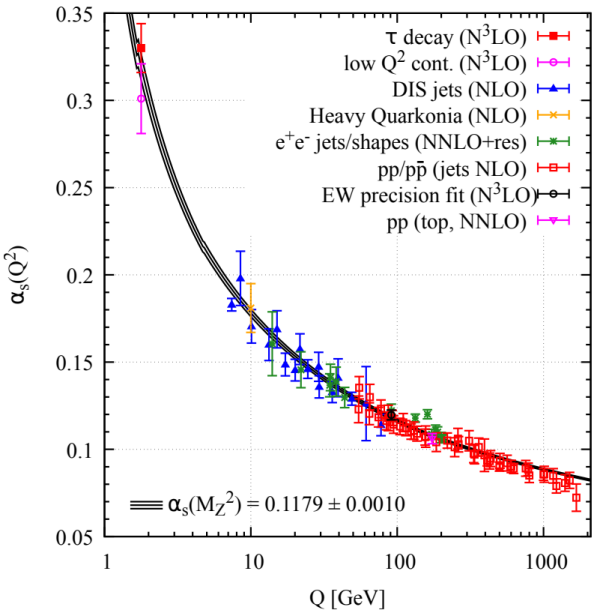
0.35
0.3
0.25
0.2
0.15
0.1
0.05
1
10
100
1000
Q [GeV]
$\alpha_s(Q^2)$
τ decay (N^{3}LO)
low Q^2 cont. (N^{3}LO)
DIS jets (NLO)
Heavy Quarkonia (NLO)
e$^+$e$^-$ jets/shapes (NNLO+res)
pp/pp̄ (jets NLO)
EW precision fit (N^{3}LO)
pp (top, NNLO)
$\alpha_s(M_Z^2) = 0.1179 \pm 0.0010$

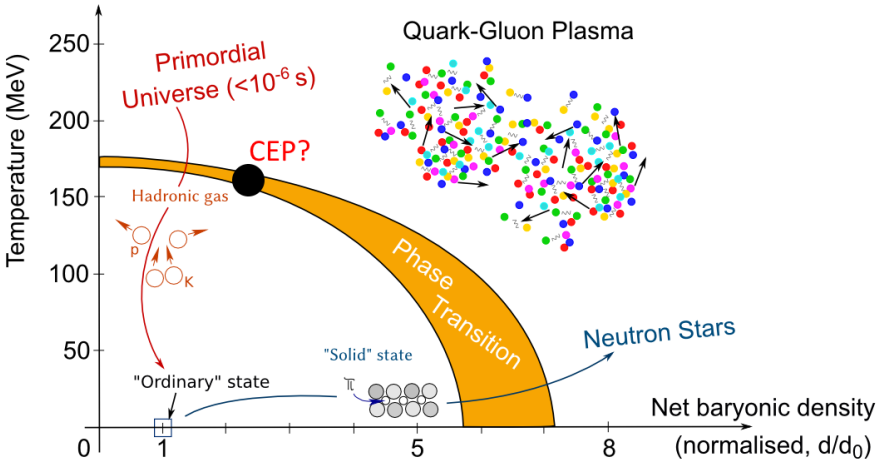
Quark-Gluon Plasma
Primordial
Universe (<10-6 s)
CEP?
Hadronic gas
p
K
Phase
Transition
Neutron Stars
"Solid" state
"Ordinary" state
Temperature (MeV)
250
200
150
100
50
0
1
5
8
Net baryonic density
(normalised, d/d0)

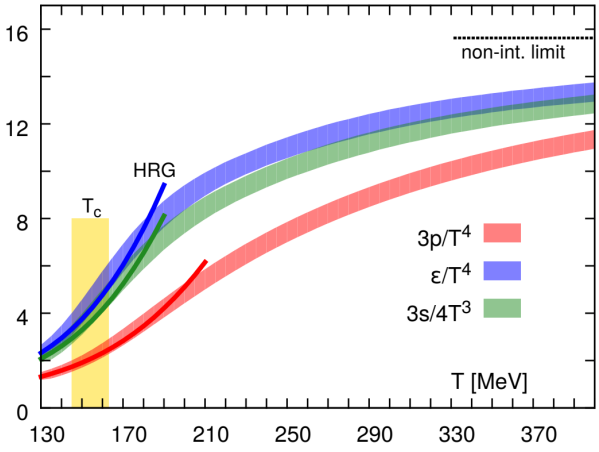
16
12
8
4
0
130
170
210
250
290
330
370
non-int. limit
HRG
T_c
$3p/T^4$
ε/T^4
$3s/4T^3$
T [MeV]

-
-

-
-

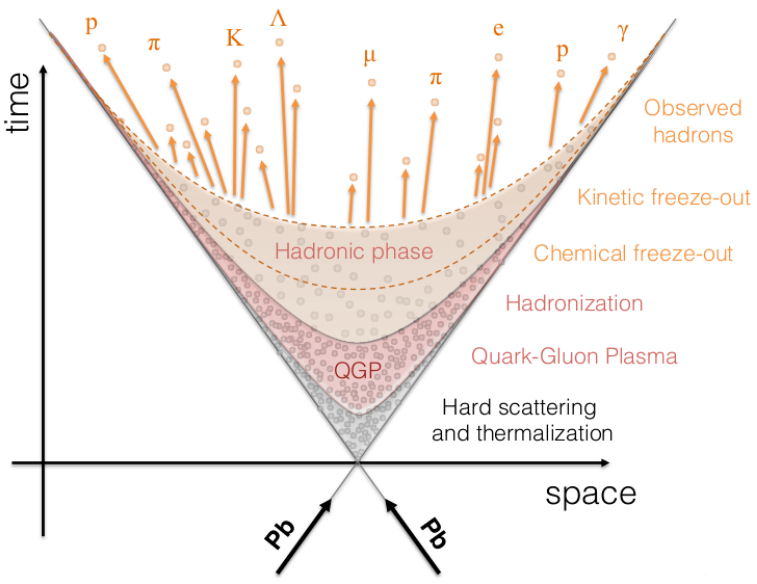
p
π
K
Λ
μ
π
e
p
γ
time
Observed hadrons
Kinetic freeze-out
Hadronic phase
Chemical freeze-out
Hadronization
Quark-Gluon Plasma
QGP
Hard scattering and thermalization
space
Pb
Pb

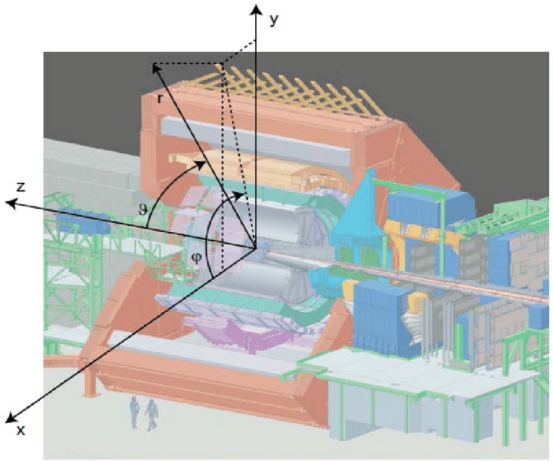
y
r
z
ϑ
φ
x

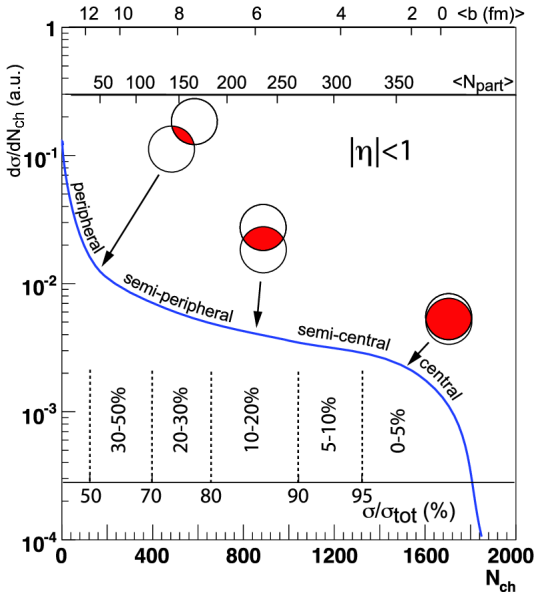
12 10 8 6 4 2 0 <b (fm)>
50 100 150 200 250 300 350 <N_part>
dσ/dN_ch (a.u.)
1
10^-1
10^-2
10^-3
10^-4
|η|<1
peripheral
semi-peripheral
semi-central
central
30-50%
20-30%
10-20%
5-10%
0-5%
50 70 80 90 95
σ/σ_tot (%)
0 400 800 1200 1600 2000
N_ch

Centrality	$dN_{\mathrm{ch}}/d\eta$	N_{part}
0 - 5 %	1601 ± 60	382.8 ± 3.1
5 - 10 %	1294 ± 49	329.7 ± 4.6
10 - 20 %	966 ± 37	260.5 ± 4.4
20 - 30 %	649 ± 23	186.4 ± 3.9
30 - 40 %	426 ± 15	128.9 ± 3.3
40 - 50 %	261 ± 9	85.0 ± 2.6
50 - 60 %	149 ± 6	52.8 ± 2.0
60 - 70 %	76 ± 4	30.0 ± 1.3
70 - 80 %	35 ± 2	15.8 ± 0.6

Table 2.1: Charged-particle multiplicity density at mid-rapidity and mean number of participant nucleons (obtained from Glauber Model estimates) for each centrality class in Pb-Pb collisions at $\sqrt{s_{\mathrm{NN}}} = 2.76$ TeV, as measured by the ALICE experiment. Data from [41].

The number of charged particles observed in the final state is much larger than the original number of participant nucleons, and decreases as the collisions become more peripheral. This should be expected, since for more peripheral collisions there is a decrease in the overlap area between the two nuclei. To study bulk particle production, it is more convenient to calculate the multiplicity *per participant pair*, as in Figure 2.4. This also allows comparisons with particle production in other collision systems, such as p-p and p-Pb. Figure 2.4 shows that multiplicity is not merely proportional to the number of participants: in the most central collisions, approximately 10 charged particles are produced for each pair of participants, while for the most peripheral ones, this number drops to about 4 particles.

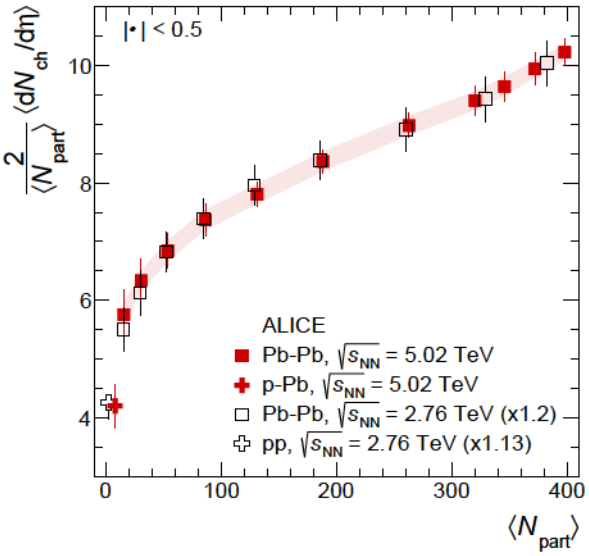

Figure 2.4: Charged particle multiplicity density in $|\eta| < 0.5$ divided by the number of participant pairs as a function of the number of participant nucleons for different collision systems. From [32].

Figure 2.4 also shows, as should be expected, that multiplicity increases with increasing collision energy, which can be seen by noticing that the data of Pb-Pb at $\sqrt{s_{\mathrm{NN}}} = 2.76$ TeV is multiplied by 1.2. From the theoretical point of view, particle production is usually described by two categories of models: two-component models which combine soft interactions and perturbative QCD processes [42, 43] and saturation models [44–46].

2.4.2 Transverse momentum distributions

Transverse momentum distributions (p_T-spectra) are also among the most commonly measured observables. A transverse momentum distribution is defined simply as a histogram counting the number of particles detected in each p_T bin, per unit rapidity. p_T-spectra contain information about the kinetic properties of the final state particles, and therefore are a powerful tool to study the bulk properties of the QGP. Figure 2.5 shows, for each centrality class, the p_T-spectra of pions, kaons and protons produced in Pb-Pb collisions at $\sqrt{s_{\mathrm{NN}}} = 2.76$ TeV, measured by the ALICE Collaboration.

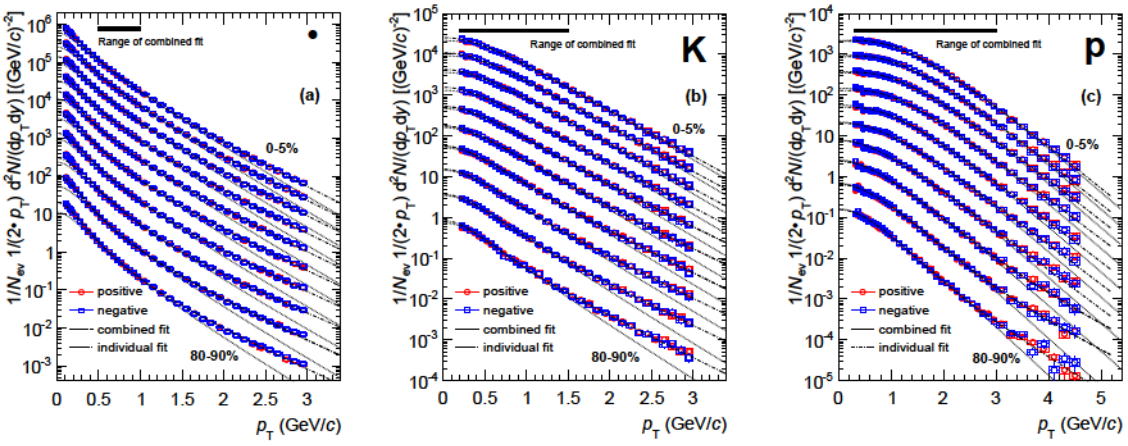

Figure 2.5: Transverse momentum distributions of pions, kaons and protons in Pb-Pb collisions at $\sqrt{s_{\mathrm{NN}}} = 2.76$ TeV measured by ALICE. From [47].

Most particles are produced at low-p_T ($p_T \lesssim 1$ GeV) and the soft region of the spectra, with $p_T \lesssim 3$ GeV, is well described by a thermal distribution. The high-p_T (hard) part of the spectra, on the other hand, exhibits a power-law behavior. Many statistical models have been employed to extract physical parameters by fitting p_T spectra [48, 49]. These include the non-extensive Tsallis statistics [50], the QCD-inspired Hagedorn inverse power law [51, 52] and the Pearson distribution [53]. A phenomenological model widely used to characterize p_T-spectra and obtain information about the kinetic freeze-out is the Blast Wave (BW) model [54], which is used in this work (see Section 5.2.4).

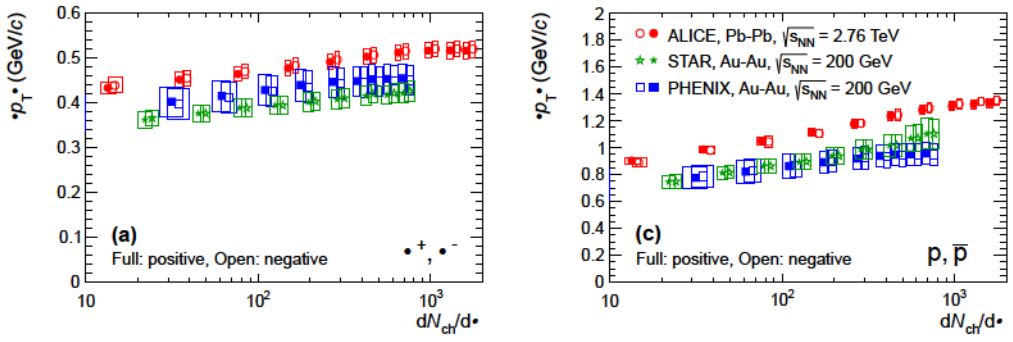

Figure 2.6: Mean p_T of charged pions (left) and protons (right) in Pb-Pb collisions at $\sqrt{s_{\rm NN}} = 2.76$ TeV and Au-Au collisions at $\sqrt{s_{\rm NN}} = 200$ GeV, as a function of multiplicity. From [47].

A straightforward quantity to extract from p_T-spectra is the mean transverse momentum of the detected particles (mean p_T):

$$\langle p_T \rangle = \frac{\int d^2p_T\, p_T \frac{dN}{d^2p_T dy}}{\int d^2p_T \frac{dN}{d^2p_T dy}} \tag{2.4}$$

Figure 2.6 shows that the mean p_T increases with multiplicity, suggesting that the transverse expansion of the system is somewhat more "violent" in central collisions.

2.4.3 Anisotropic flow

Unlike gases, where particles are far apart from each other and rarely meet, in fluids particles are constantly interacting with their neighbors, so that fluids present *collective behavior*. The experimental observation of collective behavior in relativistic heavy-ion collisions is probably the most compelling evidence that indeed a QGP is formed in such experiments. The QGP itself is never observed: collective behavior manifests itself as anisotropy in the momentum distribution of the final state particles. Due to the fact that in a non-central collision the overlap region of the two nuclei has an approximately elliptical ("almond") shape, greater pressure gradients develop in the x-direction as compared to the y-direction. In the hydrodynamic evolution, the QGP flows preferentially in the x-direction, as the fluid expands and the elliptical shape of the system becomes more circular. In this process, it is said that the spatial anisotropy is transferred to momentum space. Figure 2.7 illustrates, for a non-central collision, the time evolution of the shape of the system in the transverse plane:

As a result, more particles are detected close to $\phi = 0$ and $\phi = \pi$ and less particles are detected near $\phi = \pi/2$ and $\phi = 3\pi/2$. This momentum anisotropy in the transverse plane can be quantified by

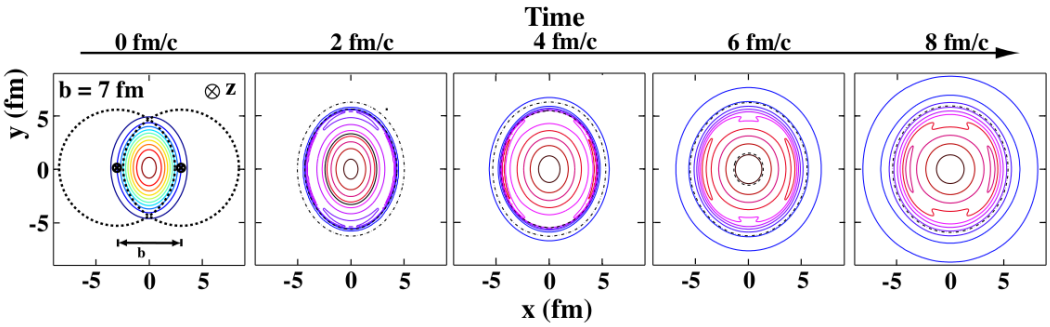
Time
0 fm/c
2 fm/c
4 fm/c
6 fm/c
8 fm/c
b = 7 fm
⊗ z
y (fm)
x (fm)
b

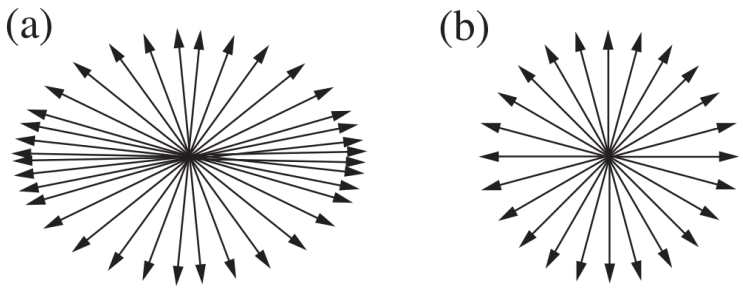
(a)
(b)

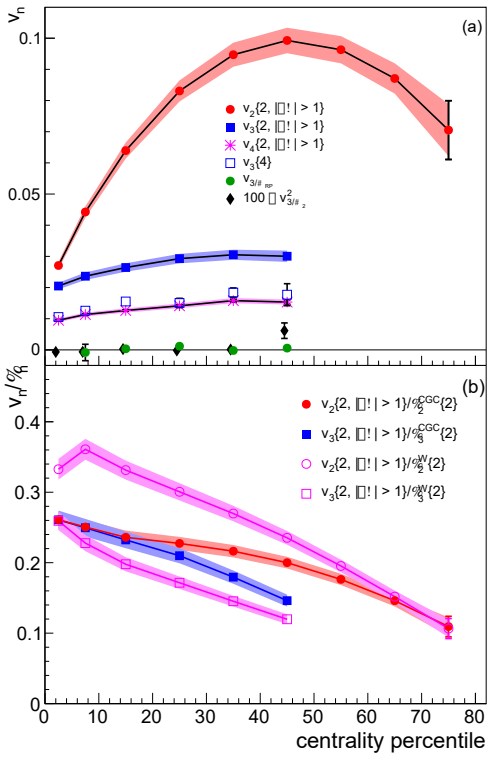
(a)
(b)
centrality percentile

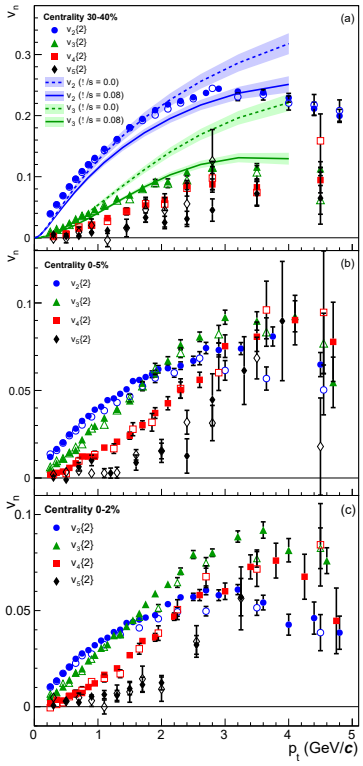
Centrality 30-40%
Centrality 0-5%
Centrality 0-2%
(a)
(b)
(c)

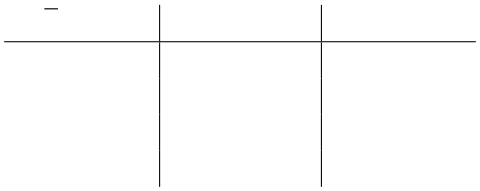

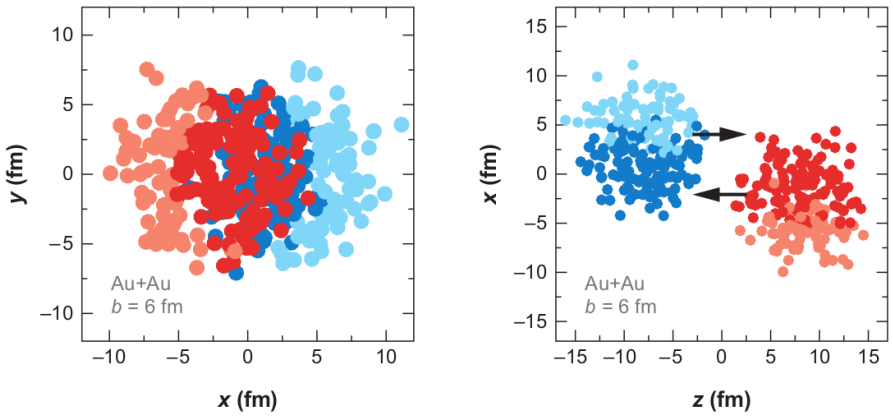
y (fm)
x (fm)
Au+Au
b = 6 fm
x (fm)
z (fm)
Au+Au
b = 6 fm

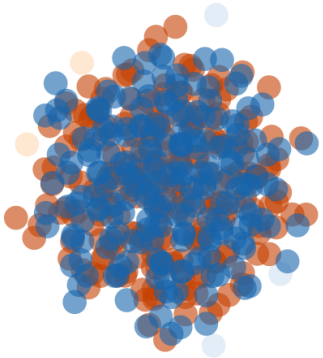

$b = 0$ fm

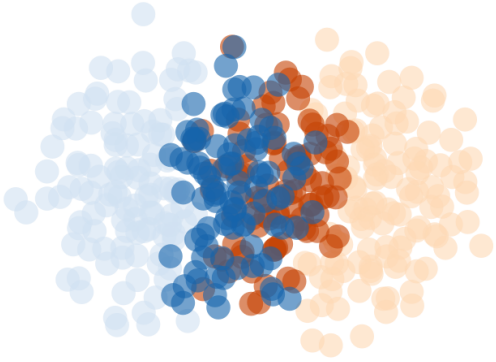

$b = 8$ fm

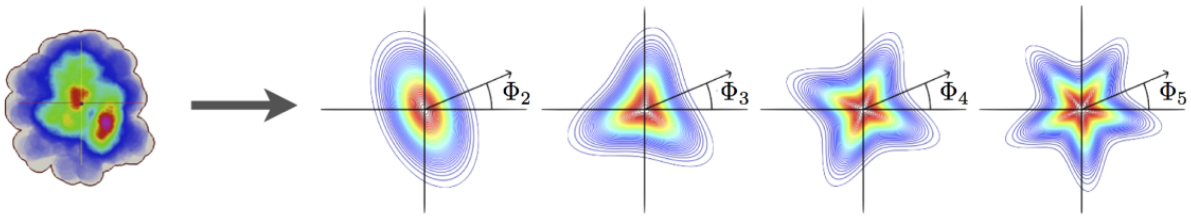

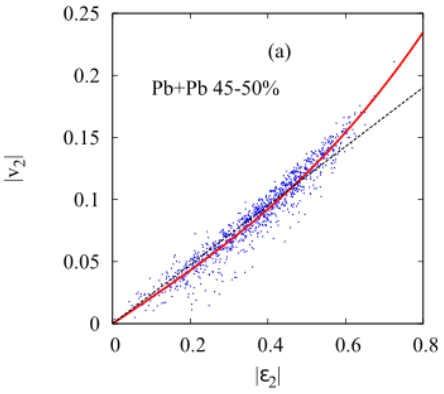
(a)
Pb+Pb 45-50%
|v2|
|ε2|
0.25
0.2
0.15
0.1
0.05
0
0
0.2
0.4
0.6
0.8

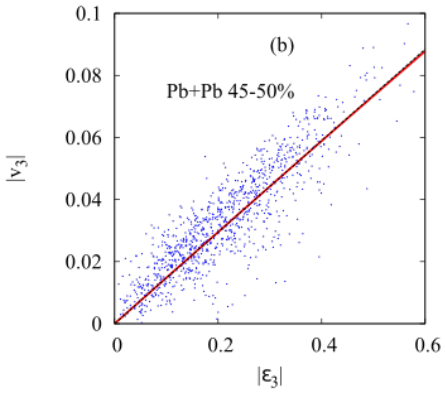
(b)
Pb+Pb 45-50%
|v3|
|ε3|
0.1
0.08
0.06
0.04
0.02
0
0
0.2
0.4
0.6

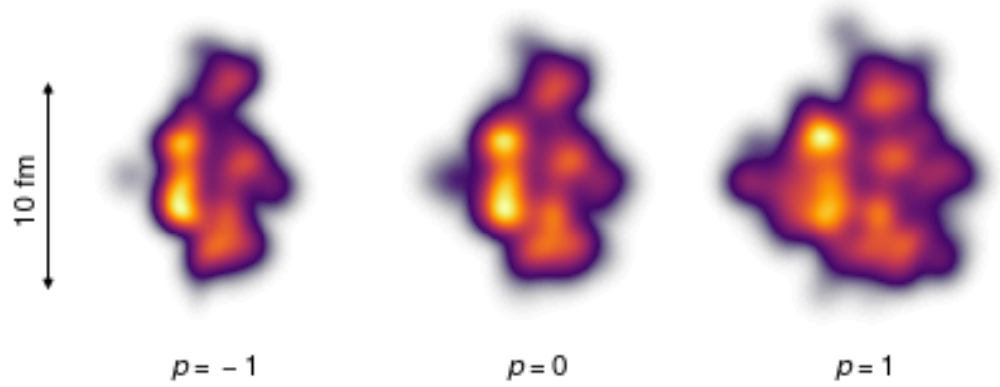
10 fm
p = − 1
p = 0
p = 1

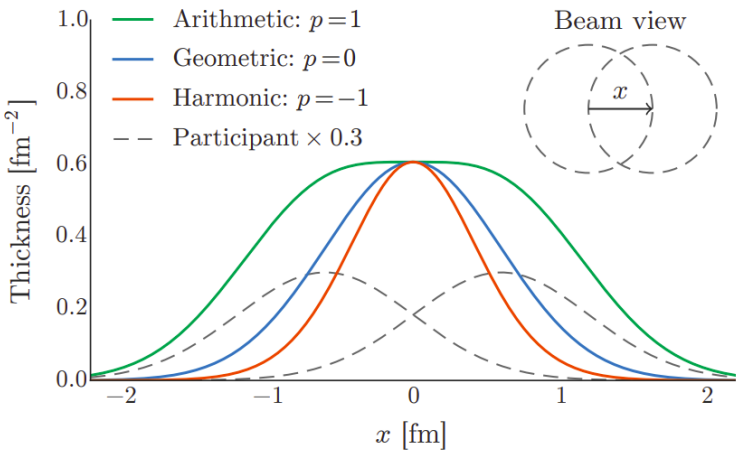
Arithmetic: $p=1$
Geometric: $p=0$
Harmonic: $p=-1$
Participant $\times$ 0.3
Beam view
x
Thickness [fm^{-2}]
1.0
0.8
0.6
0.4
0.2
0.0
−2
−1
0
1
2
x [fm]

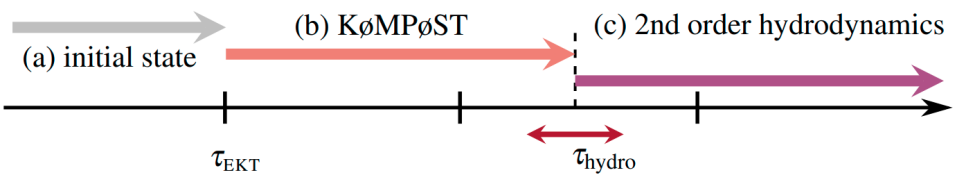
(a) initial state
(b) KøMPøST
(c) 2nd order hydrodynamics
τ_{EKT}
τ_{hydro}

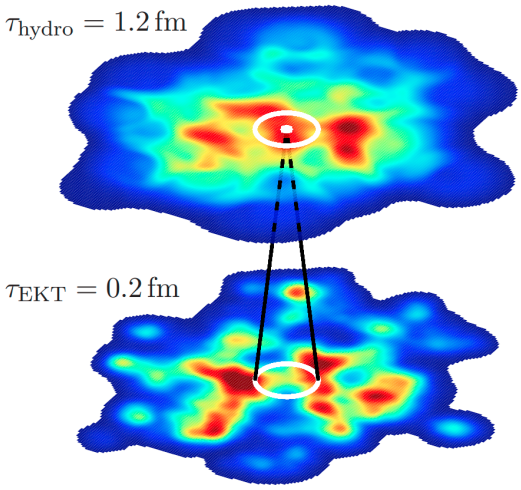
$\tau_{\mathrm{hydro}} = 1.2\,\mathrm{fm}$
$\tau_{\mathrm{EKT}} = 0.2\,\mathrm{fm}$

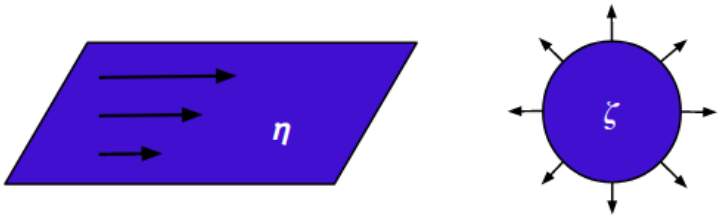
η
ζ

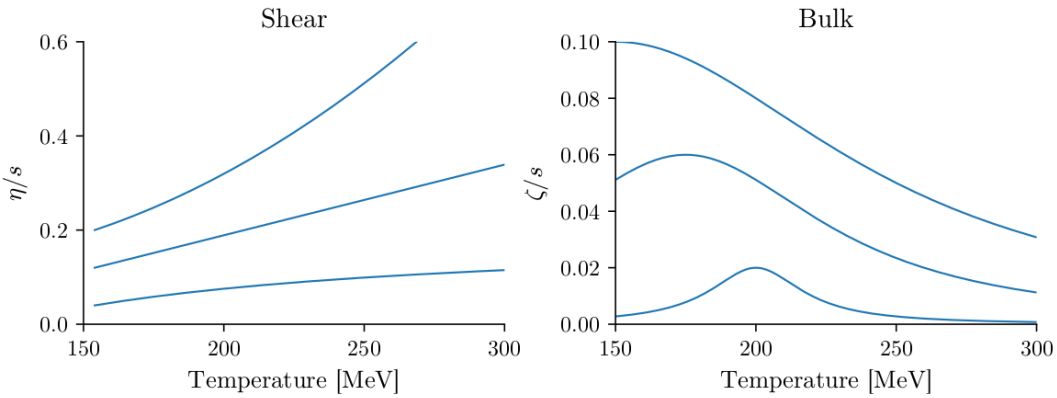
Shear
Bulk
η/s
ζ/s
0.6
0.4
0.2
0.0
0.10
0.08
0.06
0.04
0.02
0.00
150
200
250
300
Temperature [MeV]
Temperature [MeV]

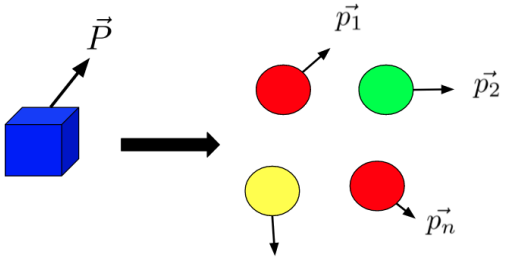
$\vec{P}$
$\vec{p_1}$
$\vec{p_2}$
$\vec{p_n}$

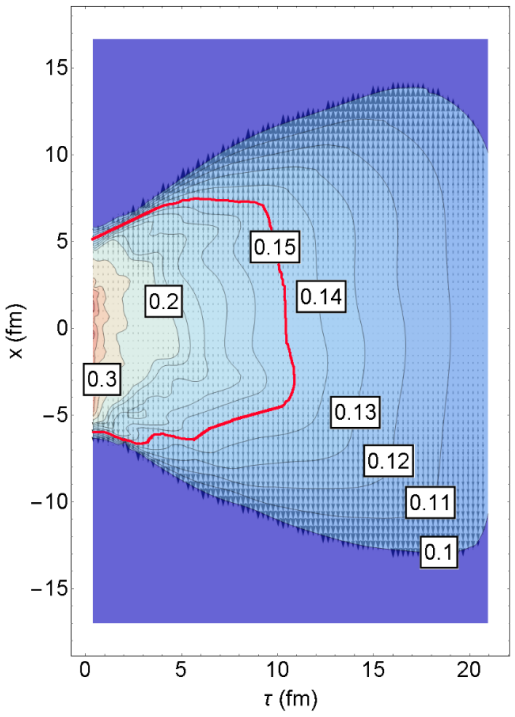
0.15
0.2
0.14
0.3
0.13
0.12
0.11
0.1
x (fm)
τ (fm)
15
10
5
0
−5
−10
−15
0
5
10
15
20

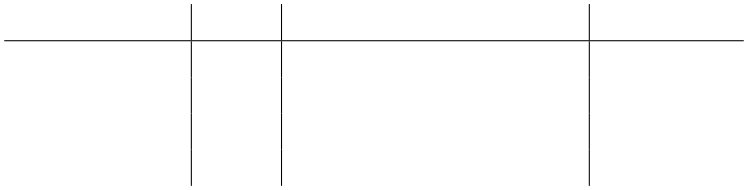

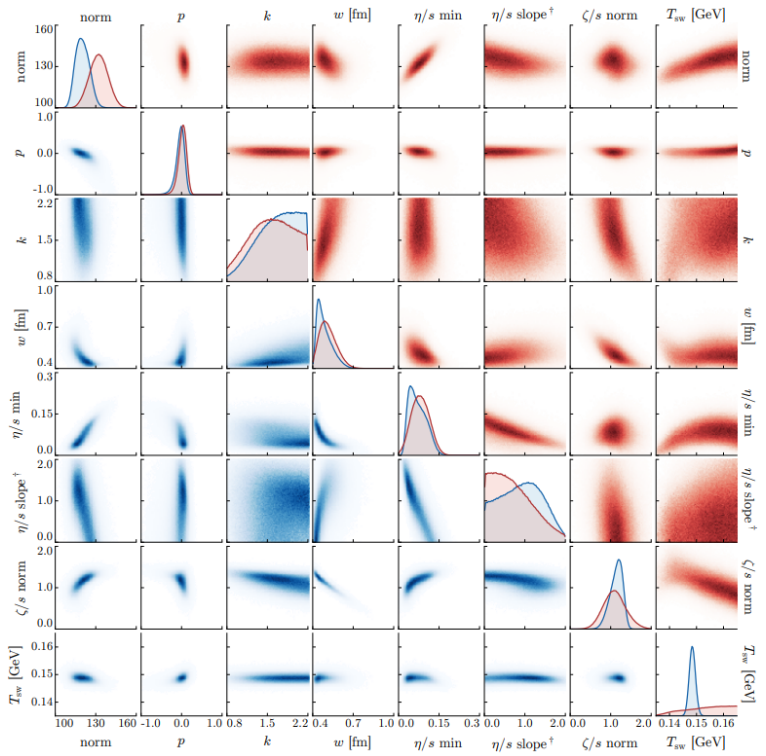
norm
p
k
w [fm]
η/s min
η/s slope†
ζ/s norm
T_sw [GeV]
160
130
100
1.0
0.0
-1.0
2.2
1.5
0.8
1.0
0.7
0.4
0.3
0.15
0.0
2.0
1.0
0.0
2.0
1.0
0.0
0.16
0.15
0.14
100 130 160
-1.0 0.0 1.0
0.8 1.5 2.2
0.4 0.7 1.0
0.0 0.15 0.3
0.0 1.0 2.0
0.0 1.0 2.0
0.14 0.15 0.16

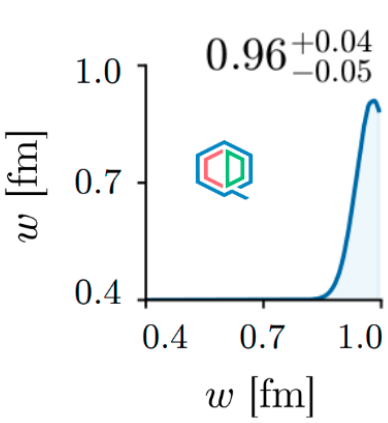
$0.96^{+0.04}_{-0.05}$
1.0
0.7
0.4
0.4
0.7
1.0
w [fm]
w [fm]

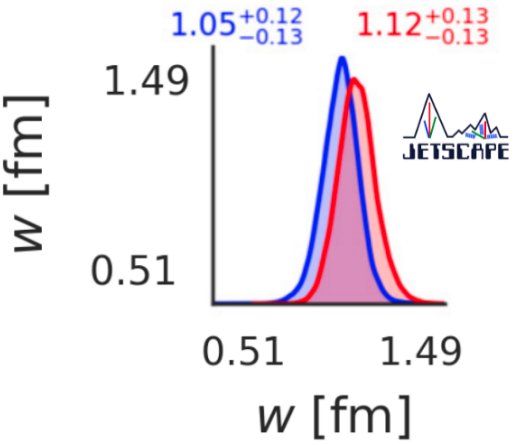
$1.05^{+0.12}_{-0.13}$
$1.12^{+0.13}_{-0.13}$
1.49
0.51
JETSCAPE
0.51
1.49
w [fm]
w [fm]

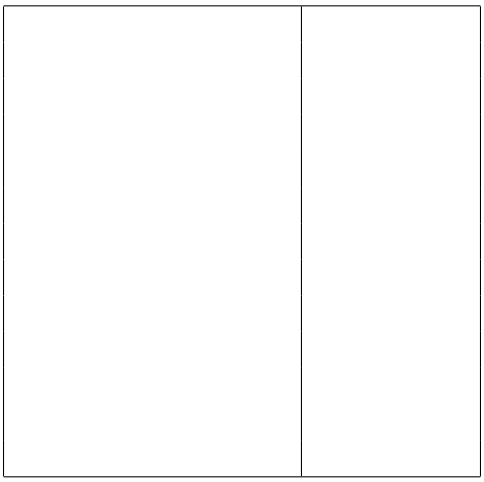

ception of the ellipticity fluctuations study, for which 10^6 events were generated in 8 impact parameter intervals (centrality classes). In Section 5.2, we present the results of the full simulation and analyze observables. In this analysis, for each value of the nucleon-width parameter, 1.000 minimum-bias (all values of impact parameter mixed together) events were generated. The centrality selection was made after that, based on the total entropy of the initial conditions.

5.1 Characterizing the initial condition

The main objective of this work is to study the impact of the nucleon-width parameter on final observables. We begin this task first by analyzing how the nucleon size affects the general characteristics of the initial condition generated by TRENTo. There is a strong relation between the initial condition characteristics and observables, so that many of the effects of the nucleon-width parameter on final state observables can be anticipated (at least in approximation) by analyzing its impact on the initial state.

We begin our investigation first by visualizing the initial condition. Figures 5.1 and 5.2 show examples of transverse entropy density profiles $s(x, y)$ generated by TRENTo in the 0 - 5 % and 30 - 40 % centrality classes, respectively:

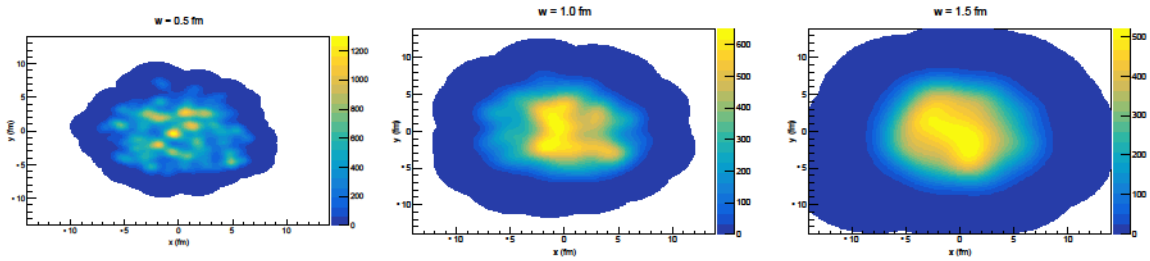

Figure 5.1: Entropy density distribution in the transverse plane of Pb-Pb collisions at $\sqrt{s_{\mathrm{NN}}} = 2.76$ TeV in the 0 - 5 % centrality class for: $w = 0.5$ fm (left), $w = 1.0$ fm (center) and $w = 1.5$ fm (right).

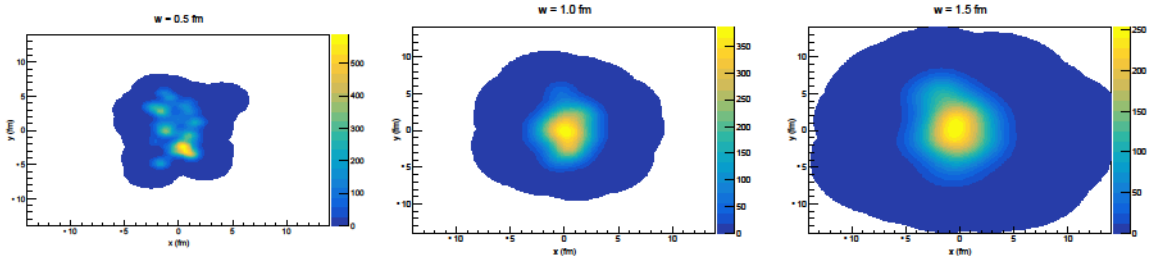

Figure 5.2: Entropy density distribution in the transverse plane of Pb-Pb collisions at $\sqrt{s_{\mathrm{NN}}} = 2.76$ TeV in the 30 - 40 % centrality class for: $w = 0.5$ fm (left), $w = 1.0$ fm (center) and $w = 1.5$ fm (right).

A straightforward visual analysis of the initial conditions suggests two most prominent effects of changing the nucleon size on the initial state:

- The system formed in the collision increases with increasing nucleon size. Furthermore, there is a decrease in system size with increasing centrality (due to the decrease of the overlap area of the two nuclei), which is more pronounced when using smaller nucleons.

- The entropy distribution's granularity ("lumpiness") decreases with increasing nucleon size. In collisions with smaller nucleons, more local high energy density regions (hotspots) can be seen in the initial condition, which gets smoother as the nucleon grows. When using the large nucleon, there is a single peak in the entropy density profile, approximately in the center of the system, which falls smoothly towards the edges of the grid.

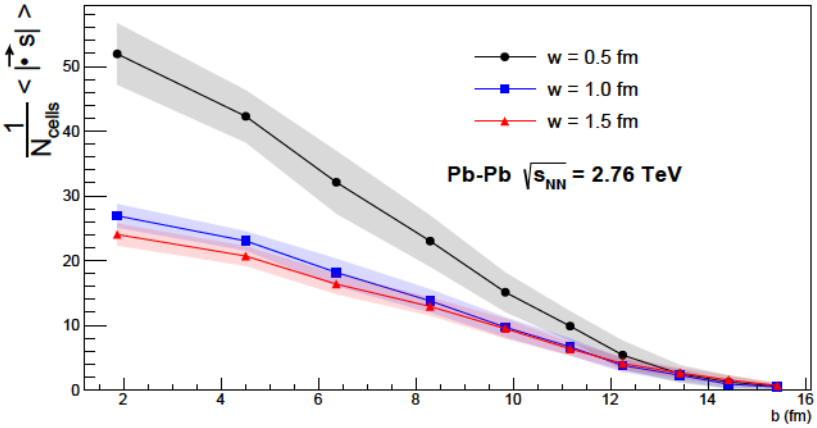

Figure 5.3: Mean gradient (per cell) of the entropy density profile calculated numerically as a function of impact parameter. Each point is the mean of 1.000 events, and the shaded region represents the event-by-event dispersion around the mean.

A visibly higher granularity of the entropy density distribution should mean stronger gradients in the initial condition. This can be verified by sweeping over all cells of the grid an calculating the gradient numerically:

$$|\vec{\nabla} s| = \sqrt{\left(\frac{\partial s}{\partial x}\right)^2 + \left(\frac{\partial s}{\partial y}\right)^2}, \tag{5.1}$$

where for each cell (i, j) we have:

$$\frac{\partial s}{\partial x} \approx \frac{s(x_{i+1}, y_j) - s(x_i, y_j)}{x_{i+1} - x_i} \tag{5.2}$$

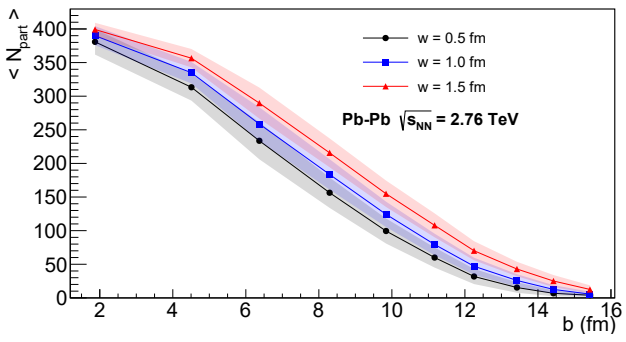
< N_part >
w = 0.5 fm
w = 1.0 fm
w = 1.5 fm
Pb-Pb √s_NN = 2.76 TeV
b (fm)

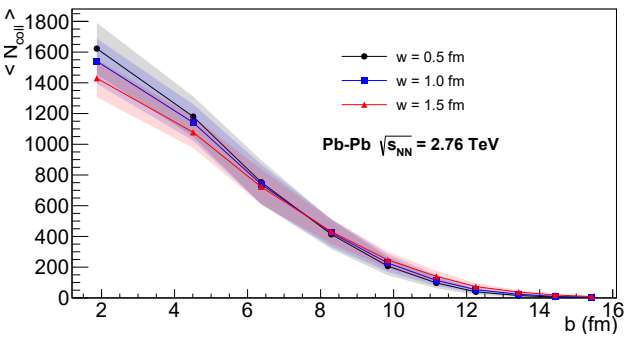
< N_coll >
w = 0.5 fm
w = 1.0 fm
w = 1.5 fm
Pb-Pb √s_NN = 2.76 TeV
b (fm)

that the collision probability used in TRENTo:

$$P_{\text{coll}}(b) = 1 - \exp[-\sigma_{gg} T_{AB}(b)] \tag{5.4}$$

depends on the nucleon size. This can be seen by substituting the Gaussian form of the thickness functions in the overlap integral:

$$T_{AB}(b) = \int dx dy \, T_A(x - b/2) T_B(x + b/2) = \frac{1}{4\pi w^2} \exp\left(-\frac{b^2}{4w^2}\right). \tag{5.5}$$

Figure 5.5 shows the functional form of Equation (5.4) as a function of the *binary collision* impact parameter, using a constant value for the effective parton-parton cross-section $\sigma_{gg} = 1$. The form of

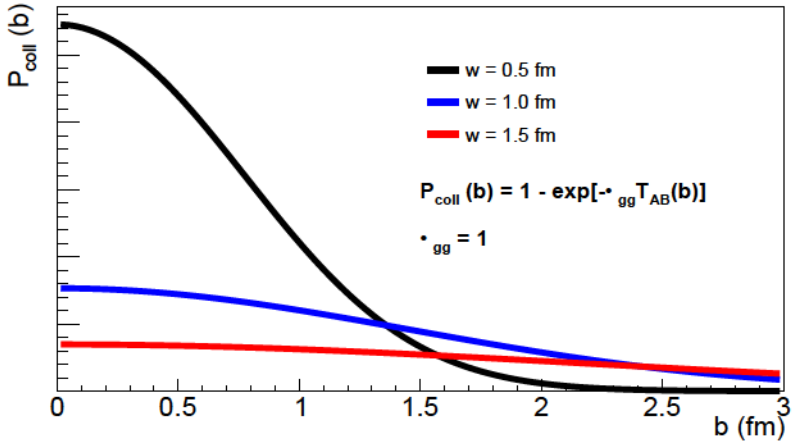

Figure 5.5: Binary collision probability as a function of impact parameter. The collision probability is more concentrated near $b = 0$ for the small nucleons.

the collision probability reflects the form of the nucleons themselves: when the nucleon-width is small, two nucleons are very likely to interact if they meet at small impact parameter, an this probability falls quickly as the impact parameter grows. As the nucleons get larger, there is a weaker dependence on the impact parameter. This explains why at small impact parameter the small nucleons collide more often, while the opposite happens in more peripheral events: the collision probability is more concentrated near $b = 0$ for the smaller nucleons. This also explains the slight increase in the number of participants as the nucleon-width increases: for larger nucleons, the collision probability is more spread, so that they are more likely to interact (at least once) when they meet at relatively large distances ($b > 2$ fm) from each other.

5.1.2 Eccentricity harmonics

A simple visual analysis of Figures 5.1 and 5.2 suggests that the geometry of the system is sensitive to the nucleon size. More quantitatively, this should manifest as a sensitivity of the eccentricity harmonics, as they are calculated using precisely the transverse entropy density distribution of the system as a weight function:

$$\varepsilon_n e^{in\Phi_n} = \frac{\int r^n e^{in\varphi} s(r,\varphi) r dr d\varphi}{\int r^n s(r,\varphi) r dr d\varphi}. \tag{5.6}$$

Figure 5.6 shows mean values of ellipticity ε_2 (left) and triangularity ε_3 (right) of the initials conditions calculated from Equation (5.6) as a function of impact parameter, considering 1.000 events generated using T_RENTo for each value of the impact parameter.

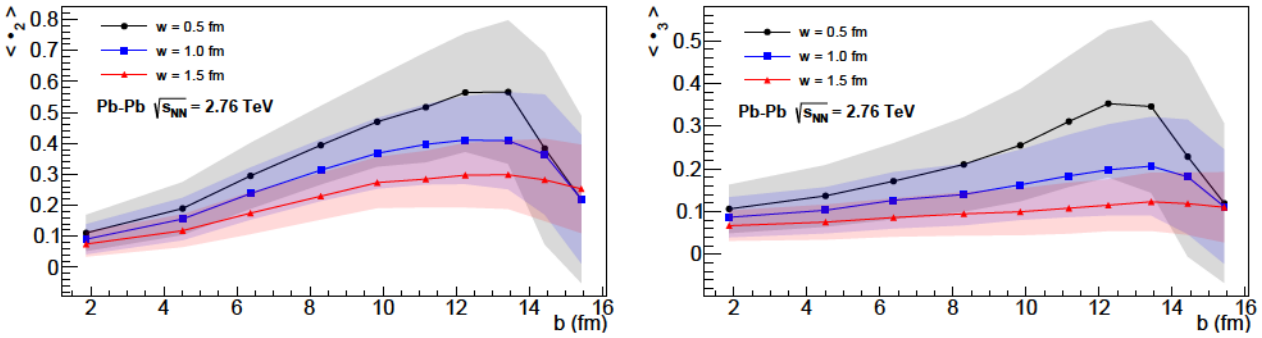

Figure 5.6: Mean value of the eccentricity harmonics for $n = 2$ (left) and $n = 3$ (right) as a function of impact parameter. Each point is the average of 1.000 events, and the shaded region represents the event-by-event dispersion around the mean.

In general, ε_2 is small in central collisions, where the overlap region between the two colliding nuclei is approximately circular. As the impact parameter grows, the overlap area acquires a more elliptical shape, and the value of ε_2 also grows. At some point, for very large values of b, the overlap area between the nuclei becomes very small (essentially created by the collision between two nucleons), and ellipticity decreases once again. This behavior as a function of impact parameter is, in general, true for higher order harmonics as well, although there is a weaker dependence with the impact parameter.

Ellipticity and triangularity are strongly affected by the nucleon size: the mean value of both eccentricity harmonics decreases as the nucleons grow larger. The smoother entropy distributions generated when using larger nucleons are more spatially isotropic. In particular, the triangular pattern is almost not present in the initial conditions generated with $w = 1.5$ fm, and there is almost no dependence on the impact parameter.

Borrowing the concept of cumulants from the flow analysis (see Section 5.2.3), we can calculate the analogous estimates for the eccentricity harmonics from cumulants:

$$\varepsilon_n\{2\} = \sqrt{\langle|\varepsilon_n|^2\rangle} \tag{5.7}$$

$$\varepsilon_n\{4\} = \sqrt[4]{\langle|\varepsilon_n|^4\rangle - 2\langle|\varepsilon_n|^2\rangle^2} \tag{5.8}$$

The ratio $\varepsilon_n\{4\}/\varepsilon_n\{2\}$ is a standard measure of event-by-event eccentricity fluctuations. Such calculations demand great statistics: in Figure 5.7, which shows ellipticity fluctuations as a function of centrality, each point was calculated using 10^6 events. Figure 5.7 shows that although the nucleon-

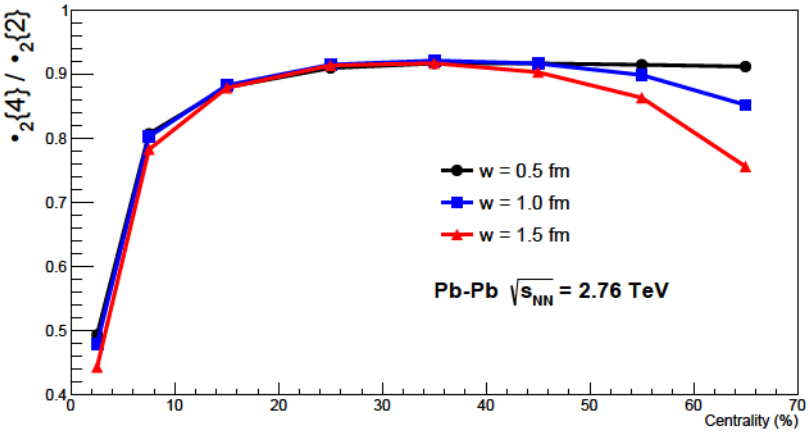

Figure 5.7: Event-by-event ellipticity fluctuations as a function of centrality. Each dot was calculated using 10^6 TRENTo initial conditions.

width strongly affects the average value of ellipticity $\langle\varepsilon_2\rangle$, there is not a strong impact on event-by-event fluctuations around the mean for more central events. For more peripheral events (from 40 - 50 % on), there is a decrease in fluctuations as the nucleon size increases. It seems intuitive that the degree of fluctuation decreases for larger values of w (as the initial conditions are smoother), and that this effect is more pronounced in peripheral events. In central events, where there are lots of binary collisions, initial conditions are more likely to "look alike" regardless of the nucleon size, while in peripheral collisions, where the system size is smaller, the effect of the nucleon size is visible.

Figure 5.8 shows the results for higher order harmonics ($n = 4$ and $n = 5$), calculated considering 1.000 events generated using TRENTo for each value of impact parameter. It is possible to see that the effects of changing the nucleon-width are even more pronounced for these higher order harmonics, for which the corresponding geometric patterns are "sharper" when compared to ellipticity and triangularity.

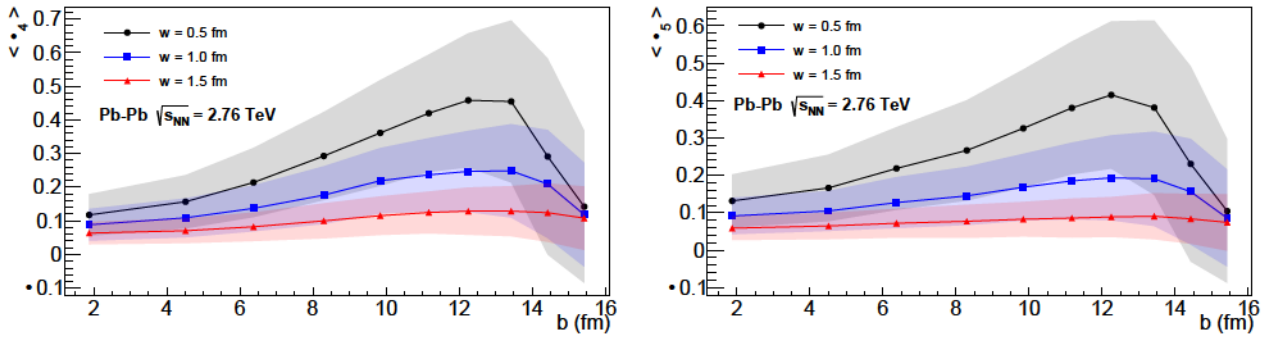

Figure 5.8: Mean value of the eccentricity harmonics for $n = 4$ (left) and $n = 5$ (right) as a function of impact parameter. Each point is the mean of 1.000 events, and the shaded region represents the event-by-event dispersion around the mean.

The results for these higher order harmonics show that indeed initial conditions generated using smaller nucleons have a more detailed and complex geometric structure, as Figures 2.1 and 2.2 suggest.

5.2 Final state observables

While Section 5.1 presented results obtained by analyzing T$_{\mathrm{R}}$ENTo initial conditions, this section presents results obtained after the complete simulation, as discussed in Chapter 3. For each value of the nucleon-width parameter, 1.000 minimum-bias (all values of impact parameter mixed together) events were generated. The centrality selection was made after that, based on the total entropy of the initial conditions (in the usual way, by ordering them from the lowest to the highest entropy values, and separating them in percentiles), which is a good predictor for the final multiplicity.

5.2.1 Charged particle multiplicity density at mid-rapidity

We begin the analysis of final state observables by calculating the charged particle multiplicity density in the mid pseudo-rapidity region ($|\eta| < 0.5$). Figure 5.9 shows charged particle multiplicity density in the region $|\eta| < 0.5$ as a function of centrality.

As seen in Figure 5.9, our results show that, in more central events, collisions with larger nucleons produce more particles, while the opposite happens for the more peripheral classes. Although $w = 1.0$ fm is essentially the MAP value of the nucleon-width in [109], a better description of the centrality dependence of charged particle multiplicity is actually obtained using $w = 0.5$ fm. In fact, until the 40 - 50 % class, the simulation using the small nucleon provides a good description (within the 10 % range) of experimental data. The simulated points were separately normalized by a constant factor so that the simulations agree exactly with experiment (and with each other) in the 20 - 30 % centrality

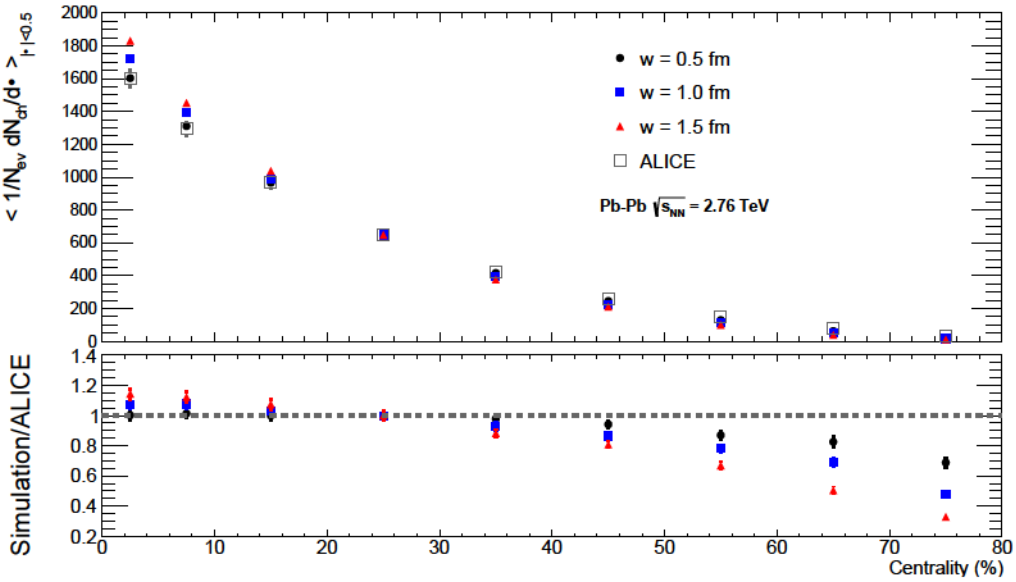

Figure 5.9: Charged particle multiplicity density in the central pseudo-rapidity region as a function of centrality. Experimental data from the ALICE Collaboration[41]. The error bars represent the event-by-event dispersion around the mean.

interval.

5.2.2 Mean transverse momentum

The stronger gradients in the initial energy density profile of the system when using smaller nucleons should have a great effect on raising the mean transverse momentum of particles in the final state of the collision. Figure 5.10 shows the mean transverse momentum of charged pions in the mid-rapidity region for Pb-Pb collisions at $\sqrt{s_{\rm NN}} = 2.76$ TeV, compared with data from ALICE. The mean transverse momentum was calculated considering the charged pions spectra from our simulation, in the $|y|$ <0.5 rapidity interval, and with $0.1 < p_T < 3$ GeV/c (to be in agreement with the experimental acceptance).

For the 0 - 5 % centrality class, the mean transverse momentum is roughly the same for the three simulations, and slightly above the experimental data (around 10 %). The simulations using the two larger nucleons provide a good description of data (within the 10 % range) across all centralities, but as events get more peripheral, the simulation with $w = 0.5$ fm generates particles with too large transverse momentum. In fact, there is an increase with centrality, which is known not to be the case.

Raising the $\langle p_T \rangle$ as a consequence of increasing the granularity of the initial condition has been well established for almost 15 years [117]. Certainly this effect is present when the nucleon size is changed, but there also seems to be more to it. To investigate this, we note there were two main

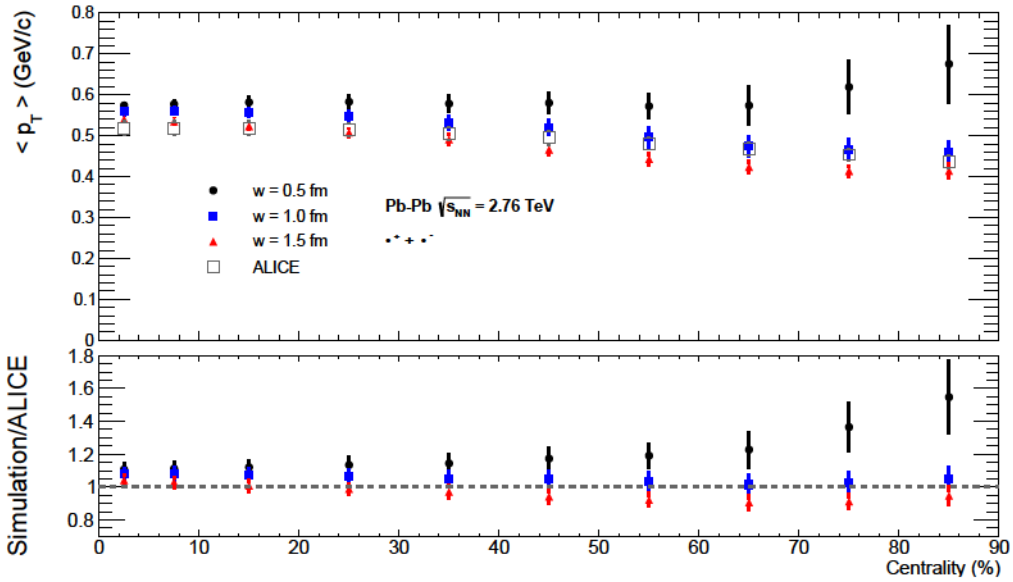

Figure 5.10: Mean transverse momentum of charged pions as a function of centrality. Data from the ALICE Collaboration [47], measured in Pb-Pb collisions at $\sqrt{s_{\mathrm{NN}}} = 2.76$ TeV. The error bars represent the event-by-event dispersion around the mean.

simplifications in the pre-equilibrium phase considered in [109]:

- In the pre-equilibrium phase, partons are assumed to be massless. Therefore, free-streaming takes place with $v = c$. This is known to result in an exaggerated large out-of-equilibrium bulk pressure when switching to hydrodynamics, which, on its turn, is responsible for an *artificially* large value of the mean transverse momentum in the final state [118].

- The pre-equilibrium phase lasts the same time for all centrality classes. As the system size decreases fore more peripheral collisions, it is reasonable to expect that the pre-equilibrium phase should last less when compared to central events (as is the case for the hydrodynamic evolution, for example). The use of a constant pre-equilibrium time results in an artificial increase of the mean transverse momentum with centrality [119], as the violent pre-hydrodynamic expansion lasts longer than it should.

The simulation using the small nucleon is the most sensitive to this second simplification in the free-streaming phase, due to the fact that the system formed is considerably smaller when compared to using the two larger nucleon-width values (Figures 5.1 and 5.2). The first simplification, on the other hand, affects all centrality classes. Figure 5.10 shows that, *in this scenario*, where the effects of the stronger gradients due to using smaller nucleons are *combined* with the effects of these two

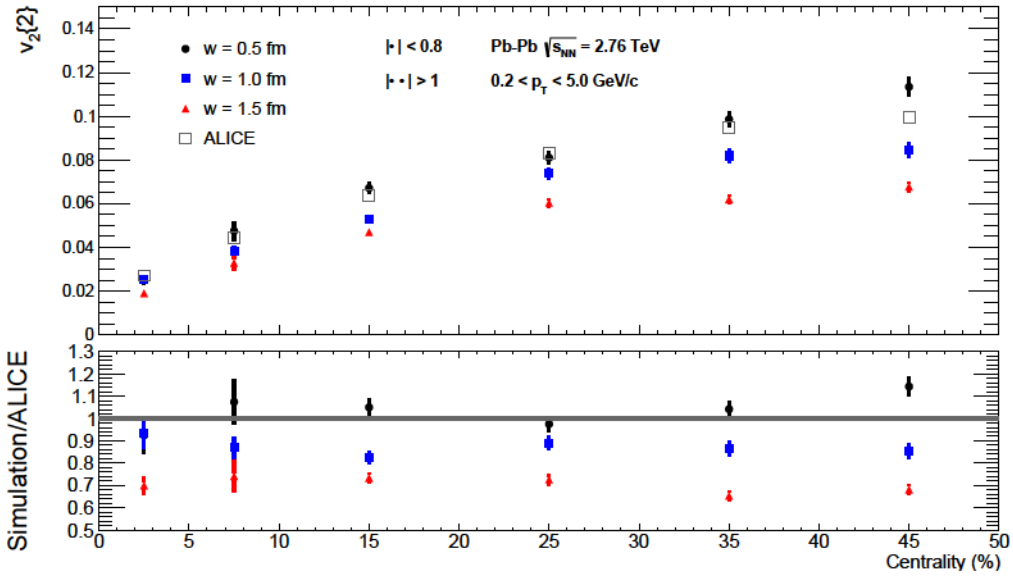

Figure 5.11: Integrated elliptic flow calculated using two-particle correlations as a function of centrality. Data from [58]. The error bars represent the event-by-event dispersion around the mean.

anisotropy mentioned in Section 2.5.2:

$$v_n = f(\varepsilon_n) + \delta_n \tag{5.23}$$

Using $w = 0.5$ fm provides a better description of data description of v_2 data (within the 10 % range), while the simulations with the larger nucleons do not produce enough elliptic flow.

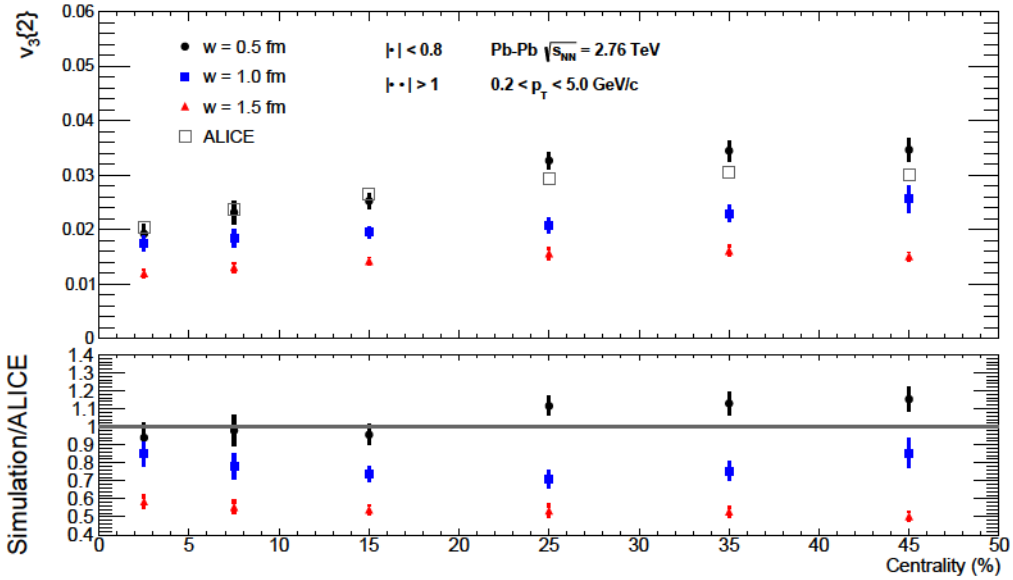

Figure 5.12: Integrated triangular flow calculated using two-particle correlations as a function of centrality. Data from [58]. The error bars represent the event-by-event dispersion around the mean.

In Figure 5.12, which shows the integrated triangular flow, this effect is even more pronounced:

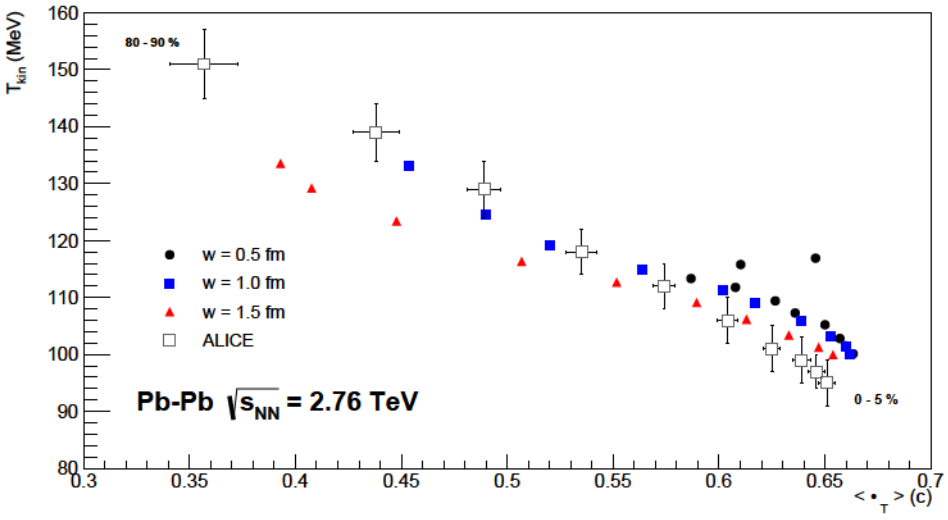

Figure 5.13: Blast Wave combined fit parameters. Each point corresponds to a centrality class. Central events are on the right, and peripheral events on the left. Data from [47].

The standard visualization of the results of a BW analysis is such as in Figure 5.13: the transverse expansion velocity is displayed in the horizontal axis and the kinetic freeze-out temperature in the vertical axis. It is clear that the simulation with $w = 0.5$ fm provides an insufficient description of experimental data, occupying a small region on the right side of Figure 5.13, while the experimental data is well spread across the plane. This suggests that, besides the mean transverse momentum, the simulation with the smaller nucleon size seems to be problematic in what concerns the description of the shape of p_T-spectra as a whole. Also, we note that for very peripheral collisions, the simulation using the small nucleons changes the trend of the transverse expansion velocity, following what was already observed in the centrality dependence of the mean transverse momentum of charged pions.

Based on our results, we conclude that the only experimental observable which constitutes the core of the Bayesian Analyses that is actually poorly described when using the small nucleons is the mean transverse momentum, which is too large. We associate this to two simplifications made in the pre-hydrodynamic stage of the simulation. In this sense, the large values of the nucleon-width parameter might have been an artefact of the Bayesian Analyses, necessary to lower the mean transverse momentum, which was being artificially raised. In addition, the combined BW fit suggests that other issues are present in the transverse momentum distributions.

ISBN

– – – –

ISBN

ISSN

[hep-ex]

–

[hep-ex]

ISSN

ISSN

ISSN

ISSN

ISSN

[nucl-ex]

ISSN

[nucl-ex]

[nucl-ex]

[nucl-ex]

[nucl-th]

[nucl-th]

[nucl-ex]

[hep-ph]

[hep-ph]

[hep-ph]

[hep-ex]

[hep-ph]

[hep-ph]

[hep-ph]

[nucl-ex]

[nucl-ex]

[hep-ph]

[nucl-ex]

[hep-ex]

[nucl-ex]

[nucl-ex]

[nucl-th]

[nucl-th]

[nucl-th]

[nucl-th]

[nucl-th]

–

[hep-ex]

[hep-ph]

[nucl-th]

[nucl-th]

[nucl-th]

[nucl-th]

[nucl-th]

ISSN

[nucl-th]

[hep-ph]

ISSN

[hep-ph]

[physics.atom-ph]

[physics.atom-ph]

[hep-ph]

ISSN

[nucl-th]

[nucl-th]

[hep-ph]

[nucl-th]

[nucl-th]

[nucl-th]

[nucl-th]

[nucl-th]

[nucl-th]

[nucl-ex]

[nucl-th]

[nucl-th]